Article

Bidirectional Power Control for a Three-Phase Grid-Connected Inverter under Unbalanced Grid Conditions Using a Proportional-Resonant and a Modified Time-Domain Symmetrical Components Extraction Method †

Mohammad Alathamneh * , **Haneen Ghanayem** and **R. M. Nelms ***

Electrical and Computer Engineering Department, Auburn University, Auburn, AL 36849, USA
* Correspondence: mqa0002@auburn.edu (M.A.); nelmsrm@auburn.edu (R.M.N.)
† This paper is an extended version of our paper published in IEEE 31st International Symposium on Industrial Electronics (ISIE), Anchorage, AK, USA, 1–3 June 2022; pp. 18–23, https://doi.org/10.1109/ISIE51582.2022.9831618.

Abstract: Discussed in this study is a bidirectional power control technique for a three-phase grid connected inverter under different unbalanced grid conditions. Prior researchers have focused on either solving the unbalanced problem or controlling the power. However, this paper addresses both issues: solving the unbalanced problems of the point-of-common-coupling (PCC) voltages and grid currents, and reducing the large ripple in the real and reactive power while also applying a bidirectional power control under weak grid conditions. A phase-locked loop (PLL) is not required because a simpler PR controller was employed. A symmetrical components extraction method was used. Compared to previous symmetrical component techniques that used complicated transformations, this approach requires less computations. Since the unbalanced load issue has been resolved, other loads connected to the grid will not be impacted. MATLAB Simulink was used in simulation experiments, and a real-time interface platform dSPACE DS1202 was used to verify the proposed control method efficacy experimentally.

1. Introduction

The need for electric power is continually increasing as modern technology develops. Consequently, sustainable energy is more important than ever. Renewable energy resource uncertainty and fluctuating load demand can weaken the AC grid and cause power quality issues such as current harmonics, unbalanced grid current problems, and unbalanced PCC voltages [1]. A three-phase quantity can be called unbalanced if there is a mismatch between the amplitude or the phases [2]. The unbalanced grid will increase the effect of the double-grid frequency component such that it can cause a ripple in the real and reactive power of the grid [3–5].

The grid-connected three-phase inverter was controlled using a variety of control techniques under balanced grid scenarios, such as proportional-integral (PI) and proportional-resonant (PR) control methods [6,7]. However, under unbalanced conditions, the PI-controller proves its deficiency with current oscillations. The PI controller has been modified in different ways to remove the current oscillation problems, such as double synchronous reference frame phase-locked loop (DDSRF PLL) in [8], direct phase-angle detection (DPD-SR) in [9], and optimum control based on DDSRF in [10]. In [11], the DDSRF method was modified and simplified by reducing the number of PLLs from two to one.

One of the most popular methods for handling power quality problems, such as unbalanced grid situations, is by using a shunt active filter approach [12]. Different shunt active power methods have been applied to balance the three-phase system and remove the ripple in real and reactive power of the grid, such as the instantaneous real and reactive power theory (PQ) [13], the conservative power theory (CPT) [14], and the synchronous reference frame method (DQ) [15]. These methods require a complicated transformation and a measurement of both voltages and currents. Another method for control of a shunt APF was proposed in [16,17] and utilized only current measurements by employing a time-domain symmetrical component extraction methodology. This approach used time delays and basic addition and subtraction to calculate the sequence components with simpler and fewer calculations.

In [18], a power controller based on a simple controller (P controller) was proposed. This method can be called the symmetrical component extraction method using the P controller (SCEM-P). The reference current consists of two parts: the balancing part (the negative/zero sequence components of the unbalanced current) and the power command current. The drawbacks of the P controller are its steady-state error and the DC offset result.

Under unbalanced grid voltage conditions, a variety of control strategies have been suggested [19–25]. Some methods attempted to balance currents when the grid voltage was unbalanced by first isolating the negative phase-sequence components of the unbalanced grid voltages. The grid impedance was estimated in [20] utilizing several control parameters, and the system parameters were defined in [21] to balance the three-phase system.

As discussed in [26–29], several techniques were employed for unbalanced current reduction, and various control situations under an unbalanced load were also explored in [30,31].

A method for using a PR controller to fix the unbalance in grid voltages produced by the unbalanced loads was presented in [32]. In microgrid systems, a notch filter was added to the virtual output impedance in order to accomplish power sharing under unbalanced loads.

In [33], it was proposed to use a modified PR control methodology to balance the grid current and power control of grid-connected inverters under unbalanced load situations. This method can be called a modified PR control strategy (MPRS). The unbalanced load operation leads to unbalanced grid currents. The controller complexity was reduced because the PR controller does not require a phase-locked loop (PLL).

The drawback of SCEM-P is the steady-state error of the P controller. However, the MPRS PR-controller showed its efficacy when dealing with unbalanced load situations. In order to control the power of the grid-connected inverter during unbalanced situations with high accuracy and low steady-state error, the approach in [34] enhanced the SCEM-P. As a result, the steady-state error of the power command was reduced while the grid current was also balanced. This method can be called the symmetrical component extraction method using a PR controller (SCEM-PR).

Prior literature has discussed bidirectional power control of grid-connected three-phase inverters under balanced grid operation, and various methods for balancing the grid in the presence of an unbalanced grid were considered without achieving power control. Few researchers talk about accomplishing both goals (balancing the grid and controlling the power) as in MPRS, SCEM-P, and SCEM-PR.

However, these three methods were applied when the grid impedance was assumed to be zero. Therefore, these approaches are applicable only under strong grid situations. In other words, the unbalanced grid currents were only considered without taking the unbalanced PCC voltages into account. In addition, power control was applied in only one direction, not bidirectional power control.

In this paper, the SCEM-PR is modified and improved to be applicable in weak grid, unbalanced situations. When the grid impedance is considered, the unbalanced cases will yield both the PCC voltages and grid currents unbalanced. The proposed method balances the grid currents and point-of-common coupling voltages, eliminates the ripple in real and

reactive power, and enables bidirectional power control in unbalanced scenarios. Results from MATLAB/SIMULINK software and experimental hardware were used to validate the suggested control technique. These results demonstrate a significant reduction in the power ripple. The unbalanced PCC voltages and the unbalanced grid currents were solved with the proposed bidirectional power control strategies.

These are the innovative contributions of this work:

- Bi-directional control of the real and reactive power under unbalanced grid situations for a three-phase inverter;
- The ripple in real and reactive power was significantly reduced;
- Balance the PCC voltages and grid currents;
- Because the unbalanced problem was solved, the unbalanced load will not have an impact on any other loads linked to the grid;
- There is no requirement for a PLL because a conventional PR controller was used;
- The symmetrical components extraction method was performed. Compared to prior symmetrical component approaches that used complicated transformations, this approach needs less computations;
- The three techniques for controlling power and balancing the grid—MPRS, SCEM-P, and SCEM-PR—described in the literature were only effective when the grid was strong and the grid impedance was ignored. Moreover, the power control was in one direction only. Here, the SCEM-PR (which is a method that takes the advantages of both SCEM-P and MPRS) was modified to control the power and balance the grid under weak grid conditions when the unbalanced grid impedance is considered.

The following is the arrangement of the paper: Section 1 discusses the introduction and literature review. Section 2 includes a description of the system model. The proposed current control method under unbalanced situations is described in Section 3, and bidirectional power control under unbalanced situations is discussed in Section 4. The performance analysis, simulation, and hardware results are presented in Section 5. Then, Section 6 summarizes the conclusions.

2. System Description

The per phase equivalent circuit of the system under study can be seen in Figure 1. The system contains a three-phase grid with grid impedance connected to the three-phase load and three-phase inverter with LCL filter at the PCC. The grid voltages V_g, PCC voltages V_{PCC}, grid currents i_g, load currents i_L, and inverter currents i_{inv} are measured.
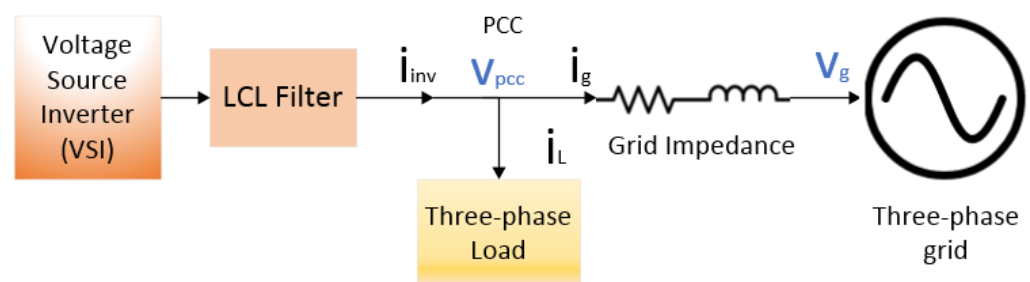
Figure 1. Grid connected three-phase inverter.

Equation (1) presents the per-phase LCL filter transfer function [16]:

$$\frac{i_{inv}(s)}{v_g(s)} = \frac{R_D C S + 1}{L_1 L_2 C S^3 + R_D (L_1 + L_2) C s^2 + (L_1 + L_2)s} \tag{1}$$

where C is the filter capacitance, L_1 is the inductance of the inverter side, L_2 is the inductance of the grid side, and R_D is the damping resistor.

Positive sequence ($f^{(1)}$), negative sequence $f^{(2)}$, and zero sequence components $f^{(0)}$ can all be obtained from any three-phase quantity. For any balanced three-phase signal, both the $f^{(2)}$ and $f^{(0)}$ sequence components are zero, while positive sequence component ($f^{(1)}$) is the only nonzero term. However, for the unbalanced signals, all of these components are non-zero. Therefore, the main cause of the unbalanced value is the presence of both negative and zero sequence components. In the proposed system of Figure 1, the grid currents will also be unbalanced when the three-phase load is not balanced. The grid current can be converted to the symmetrical components as in Equation (2):

$$i_L = i_L^{(1)} + i_L^{(2)} + i_L^{(0)} \tag{2}$$

where $i_L^{(0)}$ is the load current zero-sequence component, $i_L^{(1)}$ is the load current positive-sequence component, and $i_L^{(2)}$ is the load current negative-sequence component.

The unbalance problem was already solved in [16,17] by canceling the effect of the undesired unbalanced components. This method can be called a shunt active power filter using only current measurements (SAPF-UOCM). In this case study, it was assumed to be an ungrounded system, which means that the zero sequence component is zero ($i_L^{(0)} = 0$). Then, the unbalanced load currents can be separated into two components: the positive sequence component (the balanced part) and the negative sequence component (the unbalanced part). Balancing the system can be achieved by setting the inverter to inject the negative sequence of the unbalanced load currents as in Equation (3),

$$i_{inv} = i_L^{(2)} \tag{3}$$

This method can be expanded to cover the grounded system by setting the inverter to inject $i_L^{(2)}$ and $i_L^{(0)}$ as shown in Equation (4). Figure 2 shows the block diagram of the improved control approach:
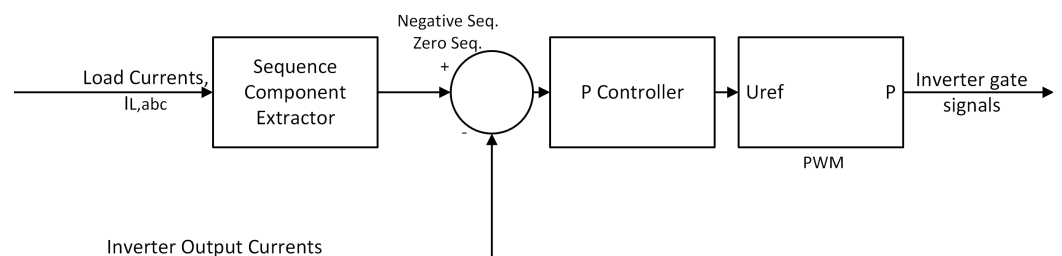
$$i_{inv} = i_L^{(2)} + i_L^{(0)} \tag{4}$$

Figure 2. The control block diagram of the improved SAPF-UOCM method.

3. Current Control

The proposed work in SAPF-UOCM was used to balance the grid without obtaining any power or current control. However, the SCEM-PR method extends the SAPF-UOCM to include current control. Any grid-connected inverter can assist in the preservation of grid current balance while transferring current and power to the grid by employing the SCEM-PR approach. The reference desired current (the power command current i_{pc}) can be added to the current equation in (4) to achieve this as shown in Equation (5):

$$i_{inv} = i_L^{(2)} + i_L^{(0)} + i_{pc} \tag{5}$$

Equation (5) can be used to control the current injected by the inverter. In order to control the current injected into the grid, Equation (6) can be used:

$$i_{inv} = i_L + i_{pc} \tag{6}$$

The three-phase inverter output current is controlled by a conventional PR controller. Equation (7) represents the PR controller's transfer function:

$$G_{PR}(s) = K_P + K_r \frac{s}{s^2 + \omega_0^2} \tag{7}$$

where K_p is the proportional coefficient, K_r is the resonant coefficient, and ω_0 is the fundamental frequency.

The reference currents and measurement currents were converted from *abc* to $\alpha\beta0$ using a Clarke transformation. Therefore, the controller needs only to be applied to two phases, as seen in Figure 3.
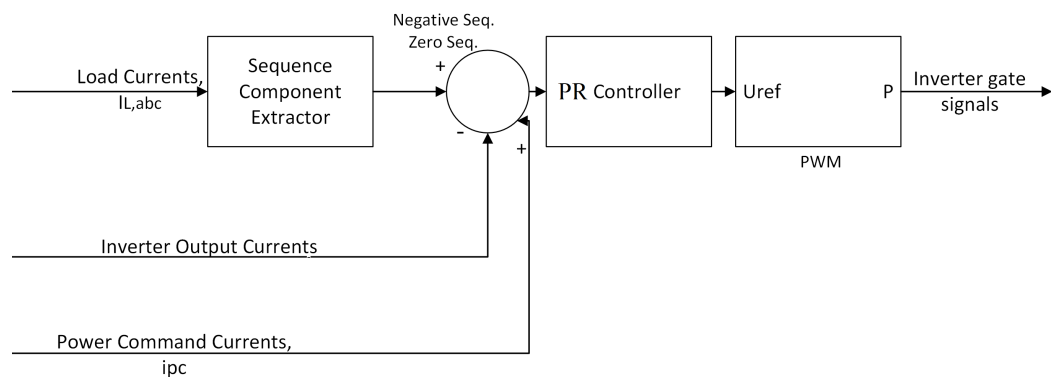
Figure 3. The current control technique using the PR controller.

The controller gains (K_p and K_r) can be tuned using reference [35] as follows:

$$K_r = K_u Im(p) \frac{\omega_u^2 - \omega_0^2}{\omega_u} \tag{8}$$

$$K_p = K_u Re(p) \frac{\omega_0^2 - \omega_u^2}{\omega_u^2} \tag{9}$$

4. Bidirectional Power Control

Real and reactive power can be controlled using the power command current component i_{pc} in Equations (5) and (6) such that, as in [36], i_{pc} can be derived using the desired real and reactive power as well as the measured PCC voltages. Equation (10) presents the real and reactive power calculation after applying the Clarke transformation and shows the importance of the PCC voltages in reference current calculations:

$$P + jQ = \left(V_\alpha i_\alpha^* + V_\beta i_\beta^* + 2V_0 i_0^* \right) \tag{10}$$

Both the grid currents and the PCC voltages will be unbalanced under weak grid conditions. Therefore, as demonstrated in Figure 4, the ripple in real and reactive power can be large.

Therefore, in order to control real and reactive power in both directions while balancing the system operation and reducing the power ripple, the i_{pc} calculation should utilize balanced components of grid currents and PCC voltages of Equation (10). The DC source of the three-phase inverter can be a combination between renewable energy sources and a battery. Therefore, the battery is able to charge and discharge allowing bidirectional power control of the inverter.
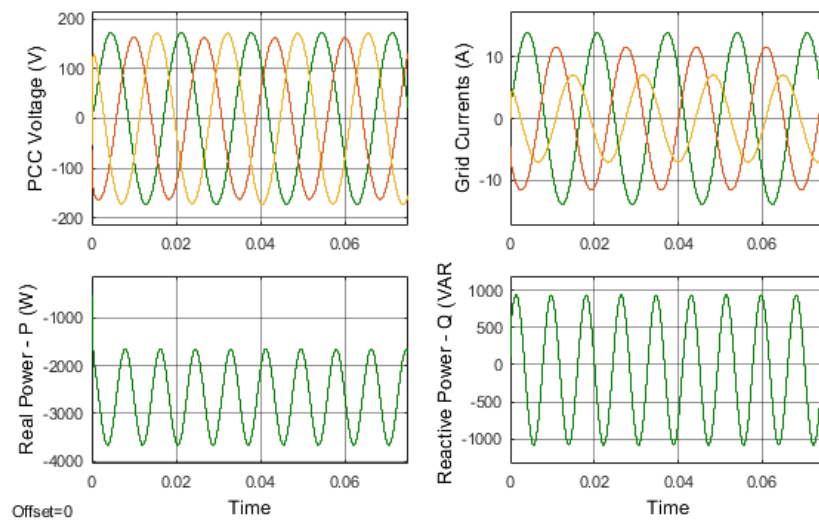
Figure 4. The ripple in real and reactive power for an unbalanced weak grid.

Equation (5) can be used to control the output power of the inverter (the injected power by the inverter to the PCC). The first two components $i_L^{(2)}$ and $i_L^{(0)}$ are associated with balancing the grid currents. Then, the V_{PCC} is the only unbalanced component. As a result, using the first approach, the injected power by inverter equals the power of unbalanced part of the load in addition to the controlled or desired power.

Equation (6) can be used to control the injected power to the grid directly. Therefore, the injected power by inverter equals the load power in addition to the controlled or desired power.

To solve the problem of unbalanced V_{PCC}, it can be converted into symmetrical components. The negative and zero sequences are associated with the unbalanced part. Consequently, the power calculation will take into account the balanced component of the PCC voltage (the positive symmetrical component of the grid voltage). The positive sequence component can be found using the symmetrical component extraction method discussed in [17]. Thus, Equation (10) can be modified to include only the positive sequence component as in Equation (11):

$$P + jQ = \left(V_\alpha^{(1)} i_\alpha^* + V_\beta^{(1)} i_\beta^* + 2 V_0^{(1)} i_0^* \right) \tag{11}$$

Using the balanced PCC voltage assumption, the term $2v_o i_0$ will be zero. Equations (12) and (13) can be obtained by simplifying the complex power equation as in [37]:

$$P + jQ = \left(v_\alpha^{(1)} i_\alpha + v_\beta^{(1)} i_\beta \right) + j \left(v_\beta^{(1)} i_\alpha - v_\alpha^{(1)} i_\beta \right) \tag{12}$$

$$\begin{bmatrix} P \\ Q \end{bmatrix} = \begin{bmatrix} v_\alpha^{(1)} & v_\beta^{(1)} \\ v_\beta^{(1)} & -v_\alpha^{(1)} \end{bmatrix} \begin{bmatrix} i_\alpha \\ i_\beta \end{bmatrix} \tag{13}$$

As a result, Equation (14) can be used to determine i_{pc} in the (alpha, beta) domain. The block diagram for determining i_{pc} is presented in Figure 5:

$$\begin{bmatrix} i_\alpha \\ i_\beta \end{bmatrix} = \frac{1}{(v_\alpha^{(1)})^2 + (v_\beta^{(1)})^2} \begin{bmatrix} v_\alpha^{(1)} & v_\beta^{(1)} \\ v_\beta^{(1)} & -v_\alpha^{(1)} \end{bmatrix} \begin{bmatrix} P \\ Q \end{bmatrix} \tag{14}$$

Figure 6 shows the overall complete block diagram of bidirectional power control for a three-phase grid-connected inverter under unbalanced grid scenarios utilizing a

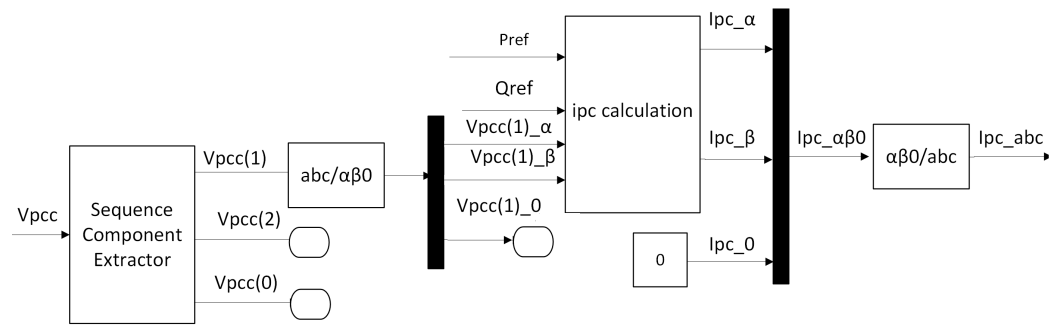modified time-domain symmetrical components extraction method and proportional-resonant controller.

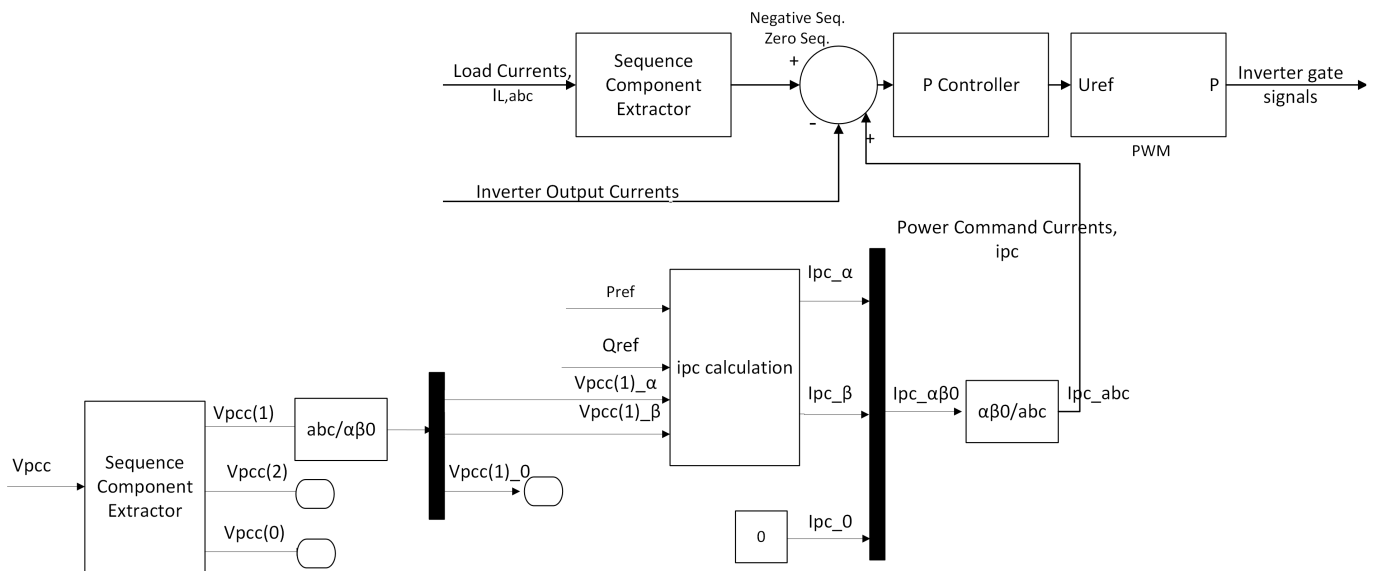

Figure 5. Power command current calculation.

Figure 6. Completed block diagram of the proposed methodology bidirectional power control under unbalanced grid conditions.

5. Case Studies

Various simulation and hardware tests were used to validate the suggested method's performance. MATLAB/SIMULINK was used to perform the simulation, and dSPACE DS1202 was utilized in the hardware experiment. The inverter is connected to the grid using an LCL filter. Figure 7 depicts the LCL filter's per phase model. The parameters of the LCL filter were designed based on [38]. The parameters for the PR controller were determined using Equations (8) and (9) and [35]. Table 1 lists the system parameters.
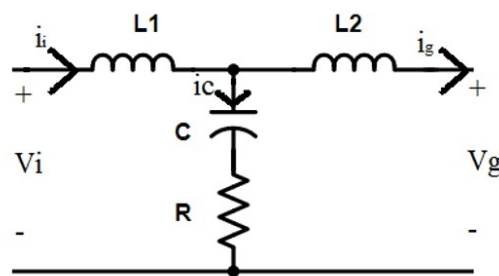

Figure 7. LCL filter per-phase model.

Unbalanced three-phase loads with $R_{a,b,c} = 8\,\Omega, 16\,\Omega$, and $32\,\Omega$ and balanced grid voltages with 120 V RMS were considered. The grid was assumed to be weak where the grid impedance was considered. Two cases of grid inductance were investigated: a balanced inductance with $L_a = L_b = L_c = 4.2$ mH and unbalanced inductance with values $L_{a,b,c} = 5.1$ mH, 4.5 mH, and $L_c = 3$ mH. Under this weak grid condition, where V_{PCC} does not equal to V_g, the unbalanced load will force both grid currents and PCC voltages grid to be unbalanced as previously mentioned in Figure 4 and Section 4.

Table 1. System parameters.

f	Grid frequency	60 Hz
V_g	Grid phase voltage	120 V RMS
f_{sw}	Switching frequency	5 kHz
V_{dc}	DC source voltage	400 V
L_1	Inverter side inductance	2.3 mH
L_2	Grid side inductance	0.58 mH
C	Filter capacitance	15 μF
R	Damping resistor	1.5 Ω
K_r	Resonant coefficient of PR controller	1800
K_p	Proportional coefficient of PR controller	2.25
$Z_{g,balanced,abc}$	Balanced grid Impedance for phases a, b, c	4.2, 4.2, 4.2 mH
$Z_{g,unbalanced,abc}$	Balanced grid Impedance for phases a, b, c	5.1, 4.5, 3 mH
R_{abc}	Three-phase load	8, 16, 32 Ω

5.1. Simulation Results

The system has been tested in simulation using MATLAB/SIMULINK model shown in Figure 8. Two cases were taken into consideration: (1) using a balanced grid impedance and (2) using i_{pc} for power control by utilizing $P_{desired}$, $Q_{desired}$, and $V_{PCC}^{(1)}$. The second approach of current control in Equation (6) was used. The injected power by inverter equals the load power in addition to the desired power. Thus, the desired power here is the injected power to the grid. The DC source of the three-phase inverter can be a combination between renewable energy sources and a battery. Therefore, the battery is able to charge and discharge allowing bidirectional power control of the inverter.
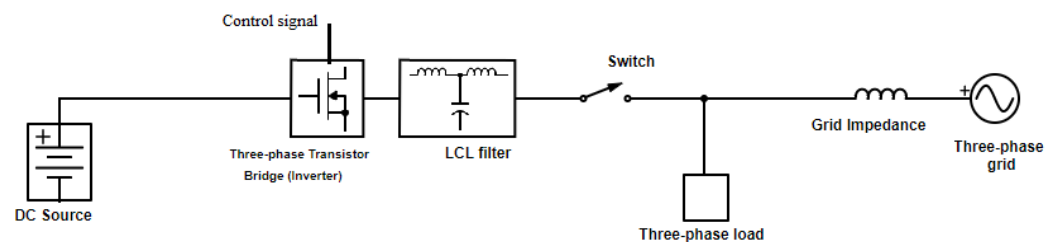

Figure 8. Test system single-line block diagram.

5.1.1. Balanced Grid Impedance

The grid inductance was assumed to be balanced with the following values: $L_a = L_b = L_c = 4.2$ mH. Figure 9 shows the the simulation results for the P and Q injected into the grid, load currents (i_L), grid currents (i_g), and inverter injected currents (i_{inv}).

1. For $t < 0.1$ s, the grid is connected only to to the unbalanced load resulting in unbalanced i_g and V_{PCC}. In addition, there is high ripple in the real and reactive power waveforms which will affect other loads linked to the PCC.
2. For $0.1 < t < 0.15$ s, the inverter was turned on and controlled as a shunt active power filter by basically assuming the power command current reference value to be zero $i_{pc} = 0$. Thus, the mode of operation is to balance the grid without controlling the power. Within a few milliseconds, the inverter can balance the grid currents, PCC voltages, and minimize the ripple in the real and reactive power.

3. For $0.15 < t < 0.2$ s, the control command has the capability to balance the system and achieve a zero desired real and reactive power to the grid (0 kW, 0 var). The proposed method can achieve this target with a small error.

4. For $0.2 < t < 0.3$ s, $(P_{desired}, Q_{desired}) = (2$ kW, -500 var$)$ while balancing the grid. The proposed method can supply the grid with the desired power as well as balance V_{PCC} and i_g.

5. At $t > 0.3$ s, the $P_{desired}$ and $Q_{desired}$ were changed to be -1 kW and 500 var. As a result, the proposed technique can control power in both directions under unbalanced grid situations.
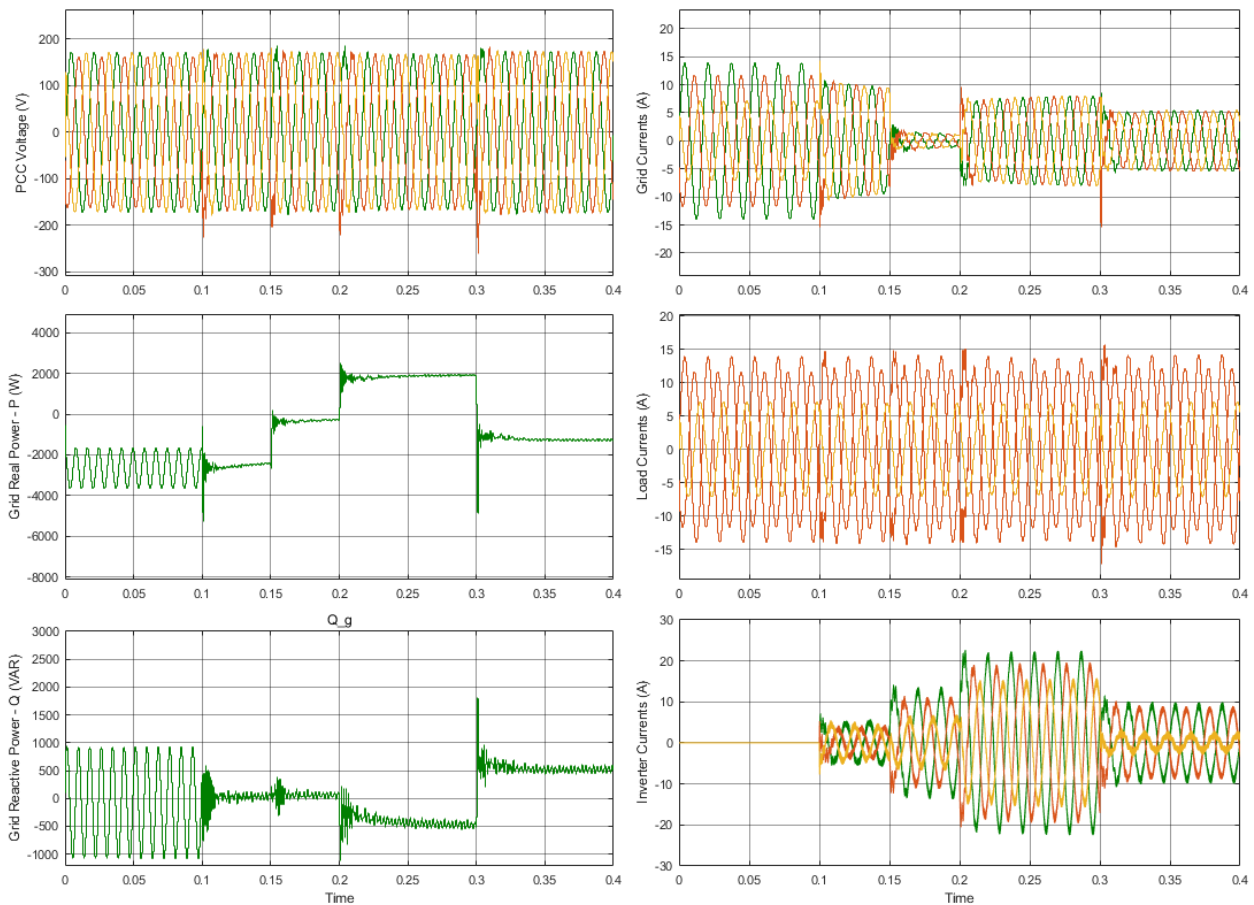
Figure 9. Simulation results under balanced grid impedance.

5.1.2. Unbalanced Grid Impedance

The grid inductance was changed to the following values: $L_a = 5.1$ mH, $L_b = 4.5$ mH, and $L_c = 3$ mH.

Figure 10 shows the the simulation results for P and Q injected into the grid, i_L, i_g, and i_{inv}.

The simulation results are very similar to the last section. For $t < 0.1$ s, the grid is connected only to the unbalanced load yielding unbalanced i_g and V_{PCC}. For $0.1 < t < 0.15$ s, the inverter was turned on and controlled as a shunt APF, so it can balance i_g and V_{PCC} and minimize the ripple on P and Q. For $0.15 < t < 0.2$ s, $P_{desired}, Q_{desired}$ were: (0 kW, 0 var). For $0.3 < t < 0.3$ s, the $P_{desired}$ and $Q_{desired}$ were modified to [2 kW, -500 var]. For $t > 0.3$ s, $(P_{desired}, Q_{desired}) = (-1$ kW, 500 var$)$.
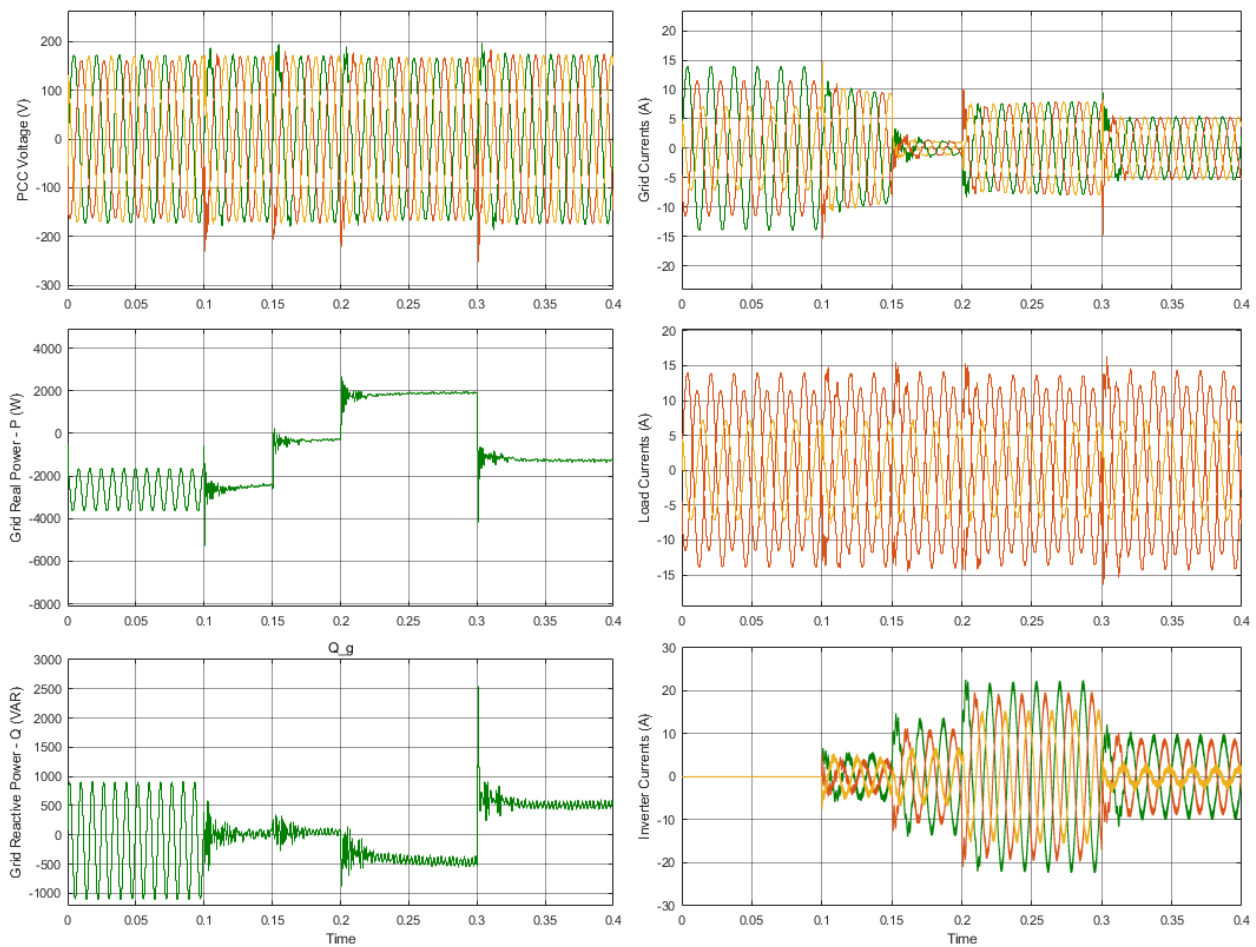
Figure 10. Simulation results under unbalanced grid impedance.

Based on these results, the proposed method proves its efficacy to balance i_g and V_{PCC}, reduce the ripple in P and Q, and bidirectional control of real and reactive power under various unbalanced situations, such as an unbalanced load and an unbalanced grid impedance.

5.2. Experimental Results

The controller was also tested in several hardware experiments. The NHR 9210 battery test system was used as a DC Source, an AgileSwitch 100 kW inverter was used as a three-phase DC-AC inverter, the NHR 9410 was used as a grid simulator, RHEOSTAT CR 9296 General Electric Co. variable resistors were used as an unbalanced three-phase load, and different current and voltage measurement boards were used to obtain the required measurements for the proposed method. A dSPACE (DS1202) real-time interface platform was used to control the inverter. Figure 11 displays the schematic diagram for the hardware connection, and Figure 12 shows the testbed system.
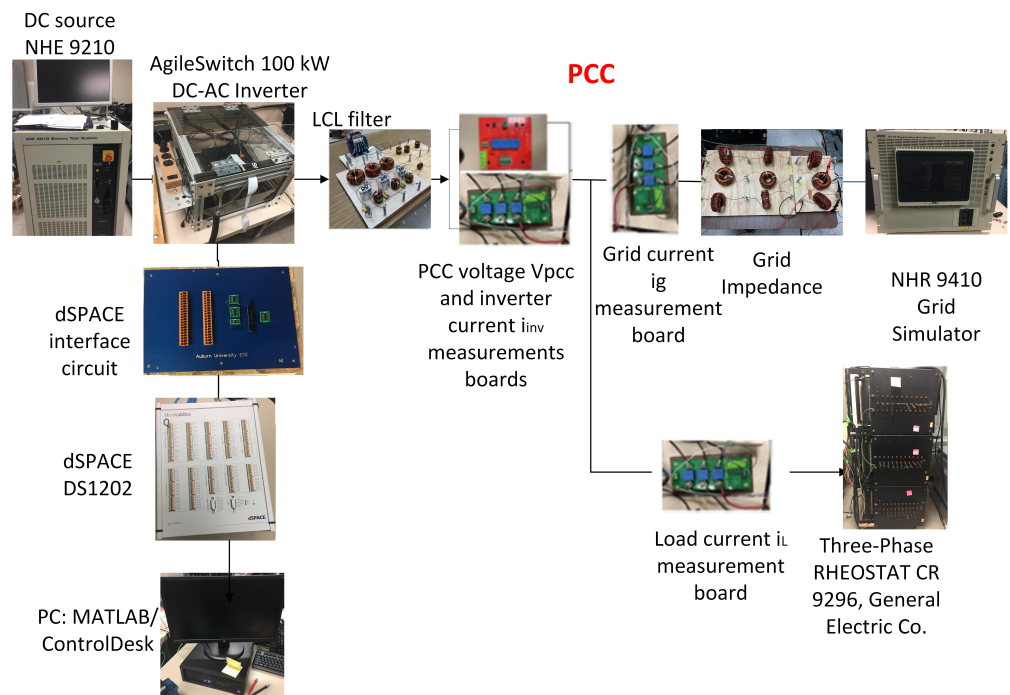
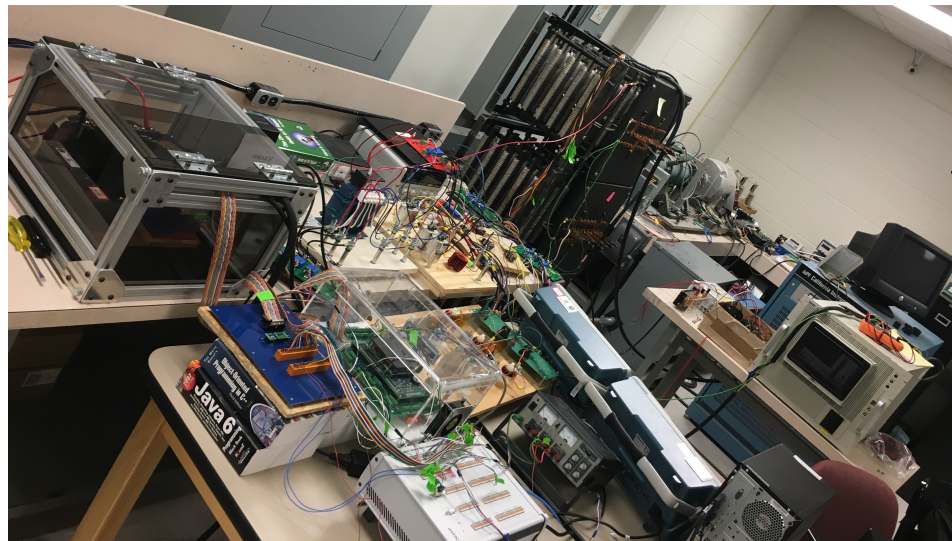**Figure 11.** Block diagram for the testbed system.

Figure 12. Hardware testbed system.

Two different experiments were performed: balanced grid inductance with values of 4.2 mH on each phase. These inductances were realized by connecting three inductors in series (1.7 mH, 1.52 mH, and 1 mH) as shown in Figure 13. For the second experiment, unbalanced grid inductors were constructed using different inductance values: 3 mH, 4.5 mH, and 5.1 mH. Three inductors were connected in series to obtain these values (3×1.7 mH = 5.2 mH, 3×15 mH = 4.5 mH and 3×1 mH = 3 mH) as shown in Figure 14. An AP300 frequency response analyzer was used to verify the accuracy of each inductor in Table 2.

Table 2. Grid inductors' parameters.

Inductance (mH)	1.7 mH	1.5 mH	1 mH
Core Type	78100-A7	77102-A7	78100-A7
Number of Stacks	3	3	2
Wire	AWG 12	AWG 12	AWG 12
Number of Turns	92	107	87
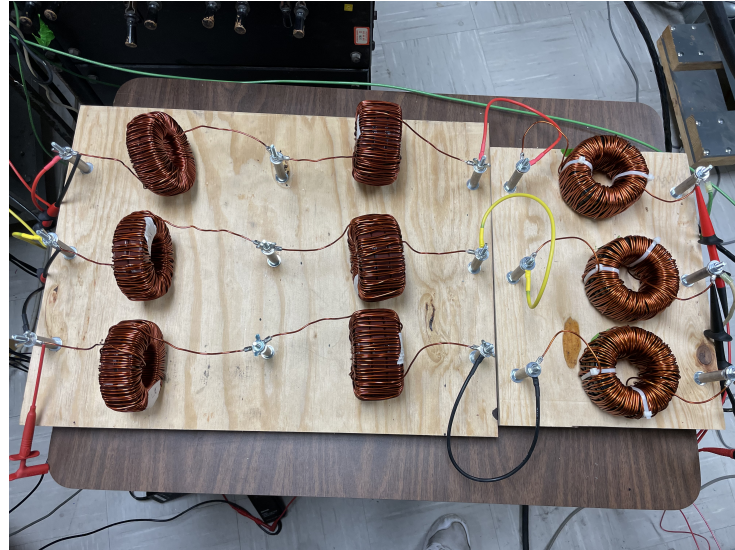
Figure 13. The balanced grid inductance with 4.2 mH.
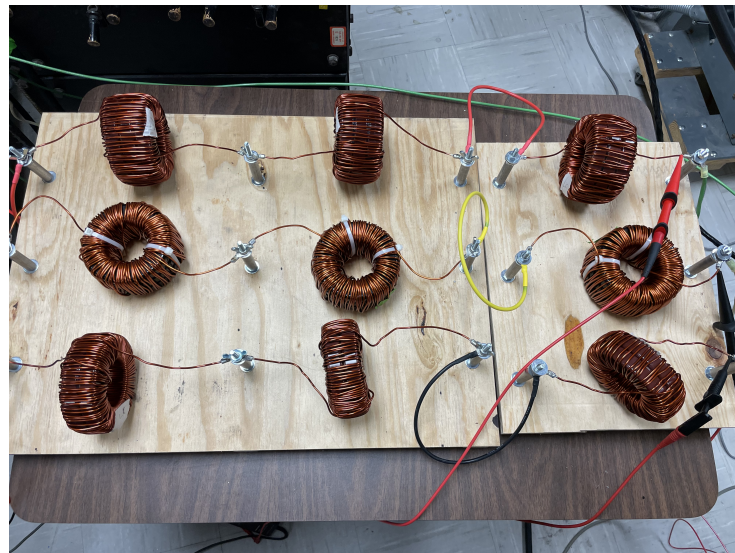
Figure 14. The unbalanced grid inductance with 5.1, 4.5, 3 mH.

The second approach of current control in Equation (6) was used. Therefore, the injected power by the inverter equals the load power in addition to the desired power. Thus, the desired power here equals the injected power to the grid.

5.2.1. Balanced Grid Impedance

Different power control cases have been evaluated as follows:

1. The unbalanced three-phase load is linked to the PCC point and the grid without energizing the inverter. At this point, the unbalanced load will create unbalanced grid currents and PCC voltages as shown in Figure 15. A Tektronix MDO3024 oscilloscope was used to obtain these results.
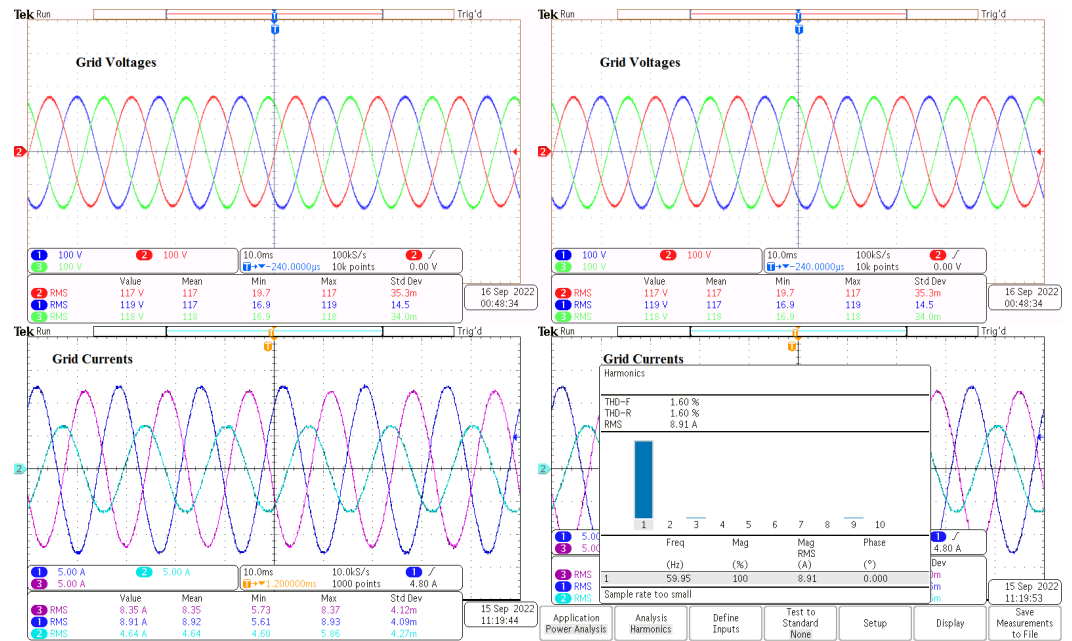
Figure 15. Experimental results before applying the proposed method under balanced grid inductances.

2. The inverter was turned on with the proposed method, and the reference P and Q are 0 kW and 0 var. The proposed method took less than 10 ms to balance the V_{PCC} and *ig* as shown in the dSPACE ControlDesk toolbox results in Figure 16. The proposed method can track the reference real and reactive power as well. Figure 17 illustrates the experimental findings for the grid voltages (V_g), PCC voltages (V_{PCC}), inverter currents (i_{inv}), and load currents (i_L) collected by a Tektronix MDO3024 oscilloscope. The experimental results utilizing the grid simulator NHR 9400 panel are shown in Figure 18.
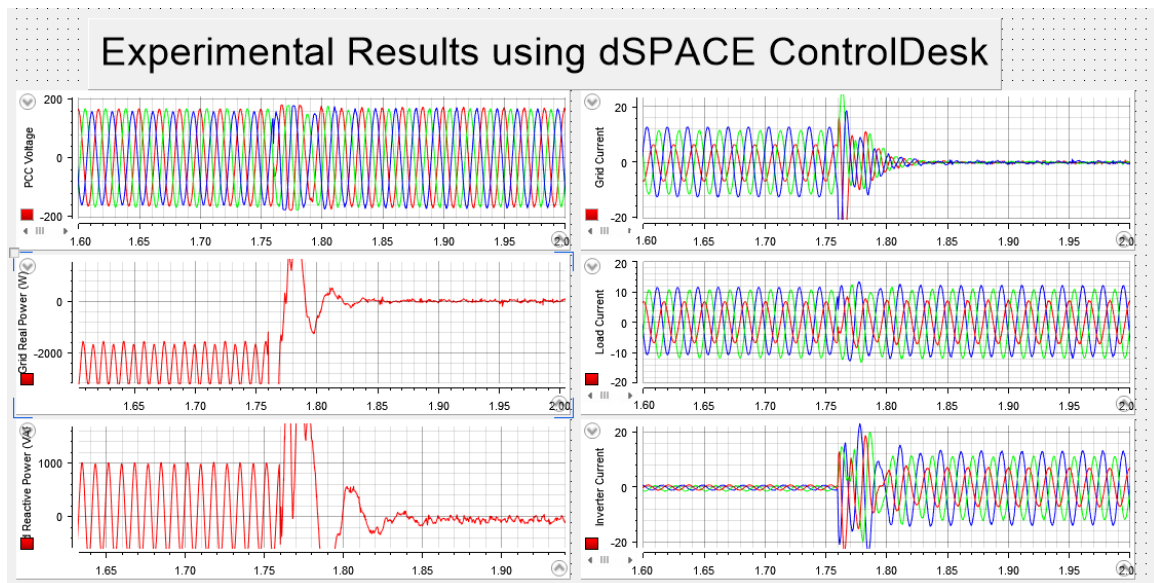

Figure 16. Hardware results using dSPACE Controldesk for real power = 0 W and reactive power = 0 var under balanced grid inductance.
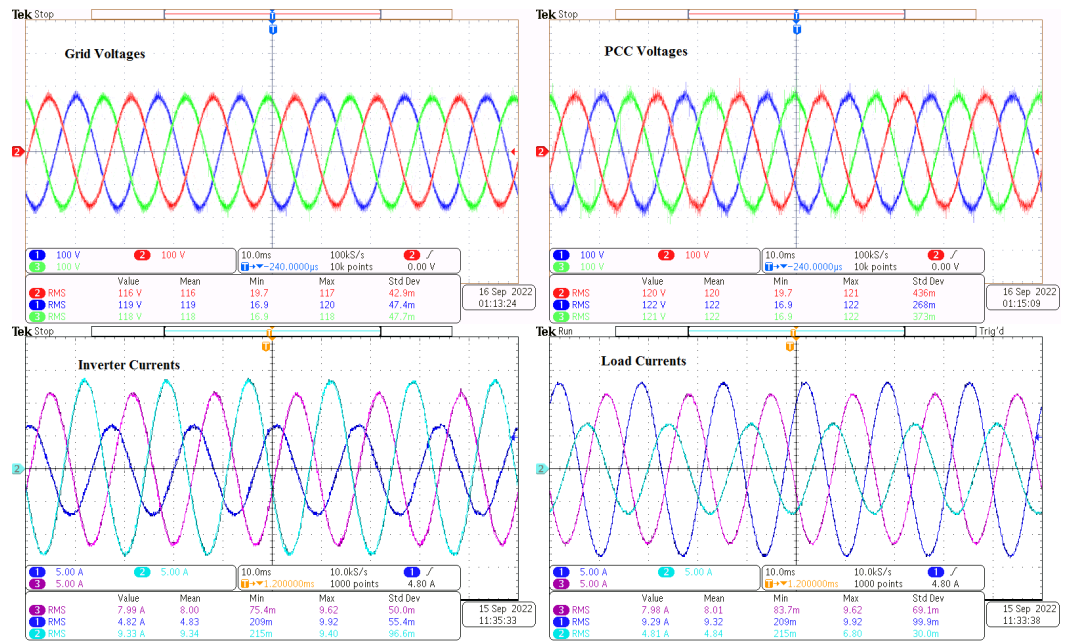
Figure 17. Hardware results using a Tektronix MDO3024 oscilloscope for real power = 0 W and reactive power = 0 var under balanced grid inductance.
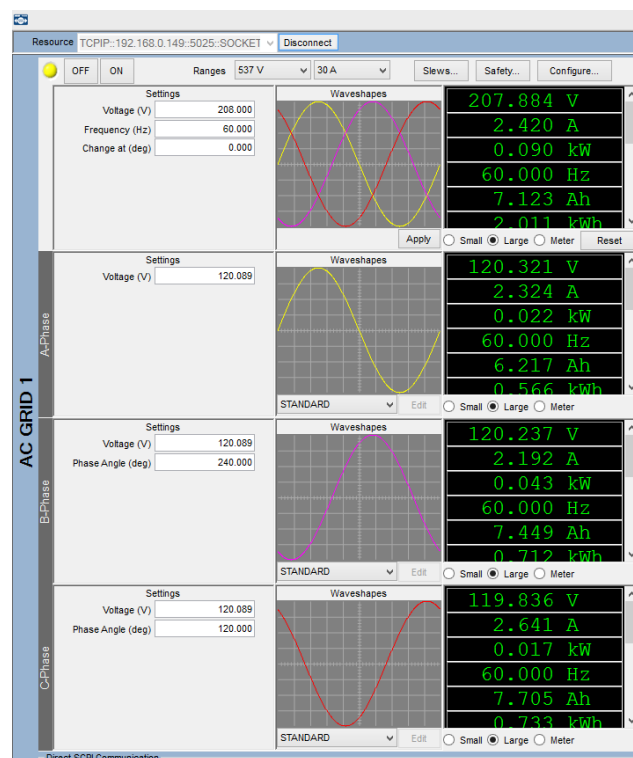

Figure 18. Hardware results using grid simulator NHR 9400 panel for real power = 0 W and reactive power = 0 var under balanced grid inductance.

3. Assuming $P_{desired} = 2$ kW and $Q_{desired} = 0$ var, the system can track the desired reference P and Q as well as balance the V_{PCC} and i_g at the same time. Figure 19 displays the dSPACE Controldesk findings, and Figure 20 shows the oscilloscope results for i_{inv}, i_L, and i_g. Grid currents have a total harmonic distortion percentage (THD%) of 2.62 %, which is regarded as an acceptable number. Although the THD% for the grid currents was 1.6% prior to energizing the inverter, the suggested method's purpose is to accomplish a bidirectional power control and eliminate the unbalance of the grid

currents and PCC voltages, improving the THD% is not a part of this work. Figure 21 displays the experimental results utilizing the grid simulator NHR 9400 panel. Note that the $P_{desired}$ direction is from the inverter to the grid, while the NHR 9400 measures the power from the grid to the inverter. Therefore, $P_{NHR,reading} = -P_{desired}$.
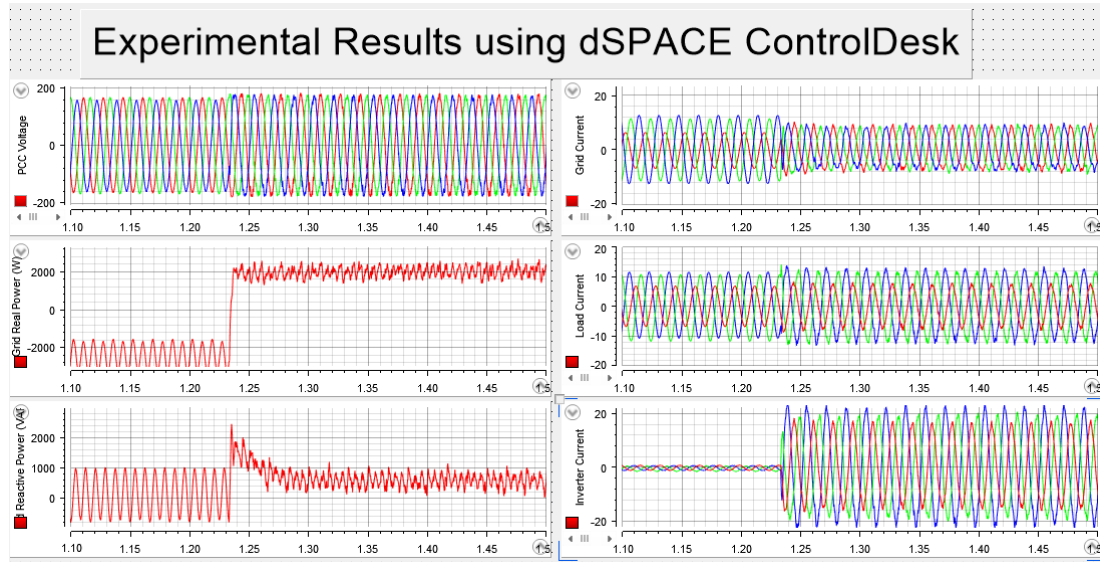

Figure 19. Hardware results using dSPACE Controldesk for real power = 2 kW and reactive power = 0 kvar under balanced grid inductances.
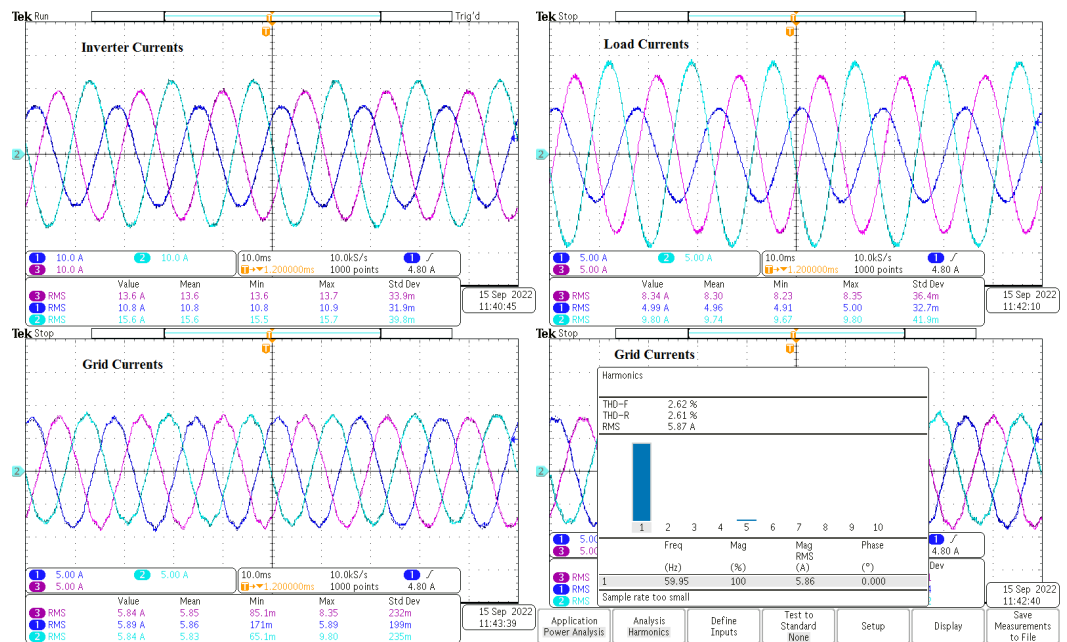

Figure 20. Hardware results using Tektronix MDO3024 oscilloscope for real power= 2 kW and reactive power = 0 var under balanced grid inductances.
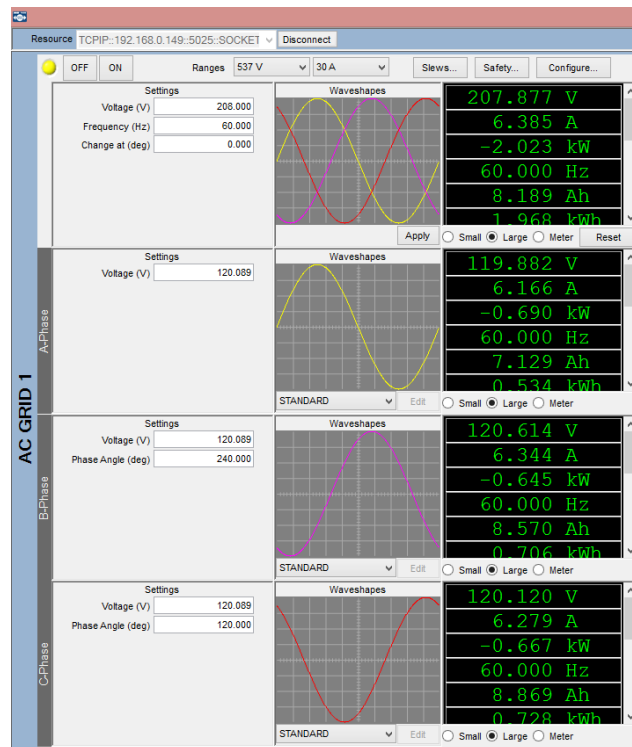
Figure 21. Hardware results using grid simulator NHR 9400 panel for real power = 2 kW and reactive power = 0 var under balanced grid inductances.

4.   At $P_{desired} = -1$ kW and $Q_{desired} = 0.5$ kvar, the suggested method can work in the four-quadrant power control mode in addition to balancing the three-phase grid currents and PCC voltages under an unbalanced three-phase load and balanced grid impedances. The experimental results using dSPACE Controldesk, oscilloscope, and grid simulator NHR 9400 are shown in Figures 22–24, respectively. The THD% value of the grid currents is 2.82%. The desired power has the opposite sign of the NHR 9400 readings ($P_{desired} = -P_{NHR\,reading}$).
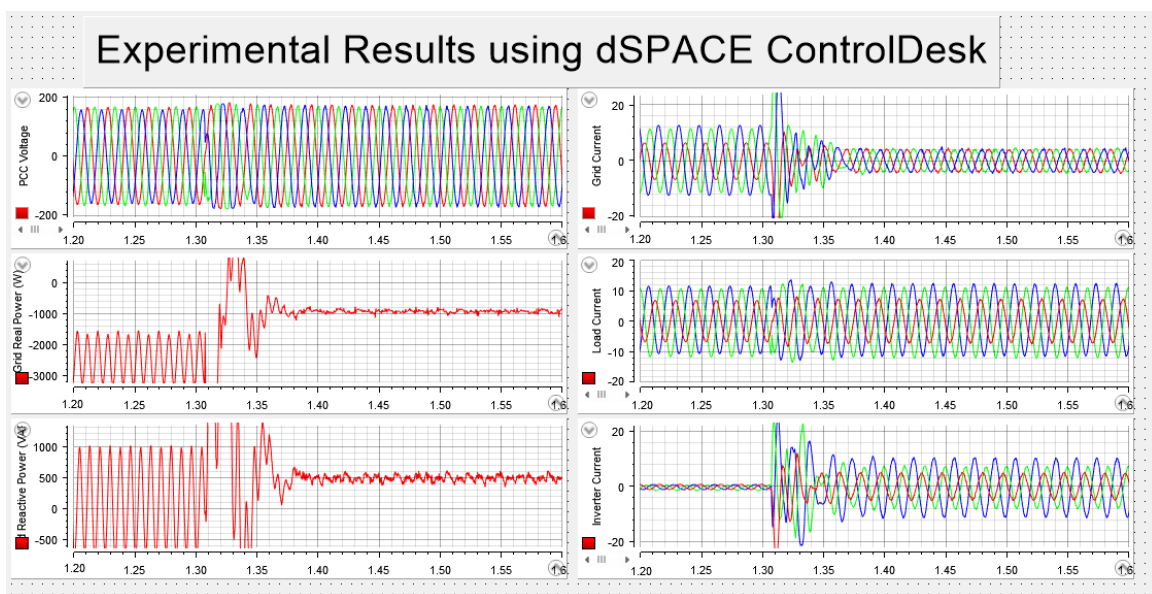

Figure 22. Hardware results using dSPACE Controldesk for real power = -1 kW and reactive power = 0.5 kvar under balanced grid inductances.
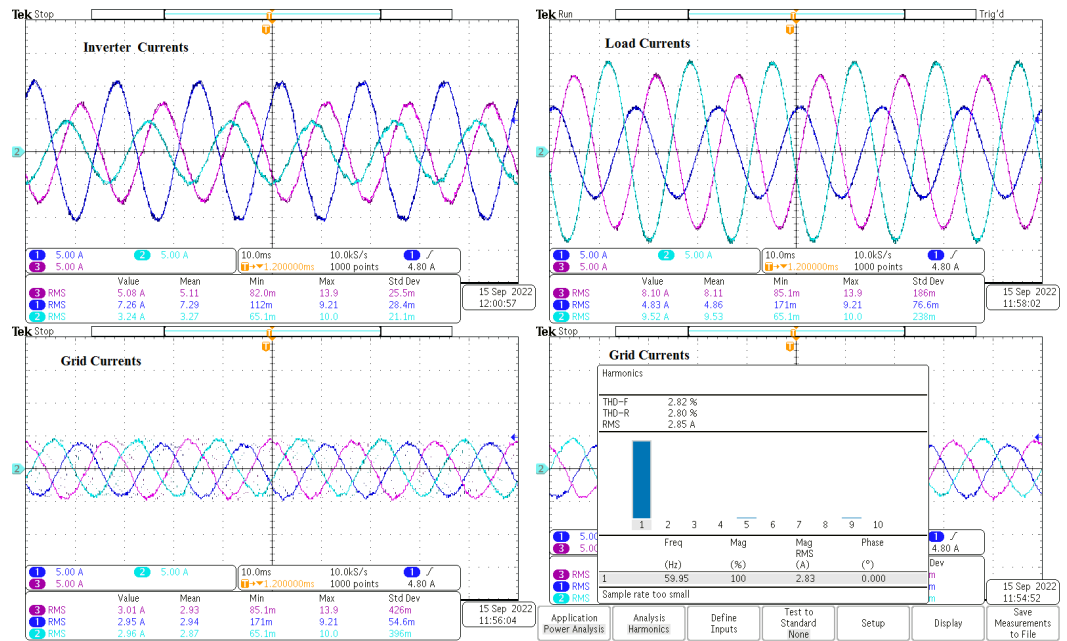
Figure 23. Hardware results using Tektronix MDO3024 oscilloscope for real power = −1 kW and reactive power = 0.5 kvar under balanced grid inductances.

Figure 24. Hardware results using grid simulator NHR 9400 panel for real power = −1 kW and reactive power = 0.5 kvar under balanced grid inductances.

5.2.2. Unbalanced Grid Impedance

The proposed method was tested as follows:

1. The unbalanced three-phase load is linked to the PCC point and the grid without energizing the inverter. At this point, the unbalanced load will create unbalanced grid currents and PCC voltages as shown in Figure 25. A Tektronix MDO3024 oscilloscope was used to obtain these results.
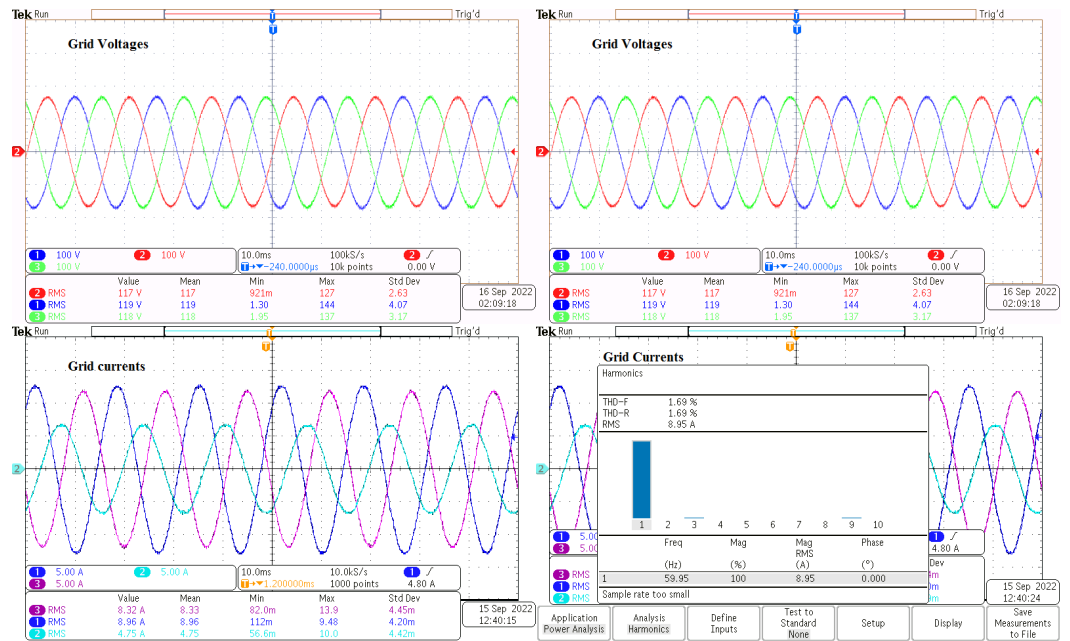
Figure 25. Experimental results before applying the proposed method under unbalanced grid inductances.

2. The inverter was turned on with $P_{desired}$ and $Q_{desired}$ equal to 2 kW and 0 var, respectively. The proposed method took a few milliseconds to balance V_{PCC} and *ig*. The system can track the desired reference P and Q as shown in the dSPACE ControlDesk toolbox findings in Figure 26. Figure 27 shows the oscilloscope results for V_g, V_{PCC}, i_{inv}, i_L, and i_g. Grid current THD% is 2.59%. Figure 28 displays the experimental results utilizing the grid simulator NHR 9400 panel. The desired power has the opposite sign of the NHR 9400 readings ($P_{desired} = -P_{NHR,reading}$).

Figure 26. Hardware results using dSPACE Controldesk for real power = 2 kW and reactive power = 0 var under unbalanced grid inductances.

Figure 27. Hardware results using Tektronix MDO3024 oscilloscope for real power = 2 kW and reactive power = 0 var under unbalanced grid inductances.
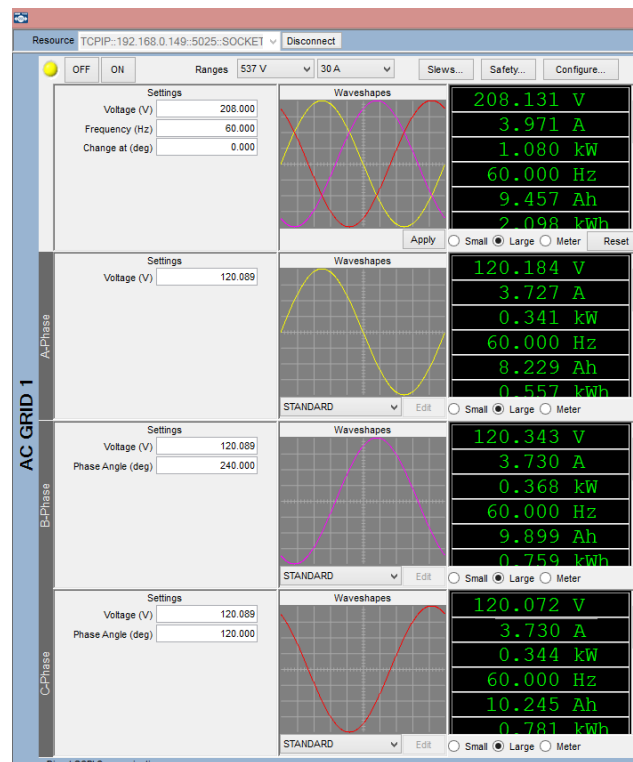

Figure 28. Hardware results using grid simulator NHR 9400 panel for real power = 2 kW and reactive power = var under unbalanced grid inductances.

3. At $P_{desired} = -1.5$ kW and $Q_{desired} = 0.5$ kvar, the suggested method can work in the four-quadrant power control mode in addition to balancing the three-phase grid currents and PCC voltages under an unbalanced three-phase load and unbalanced grid impedances. The experimental results using dSPACE Controldesk and grid simulator NHR 9400 are shown in Figures 29 and 30, respectively. The THD% value

of the grid currents is 2.3%. Note that the desired power has the opposite sign of the NHR 9400 readings ($P_{desired} = -P_{NHR\,reading}$).
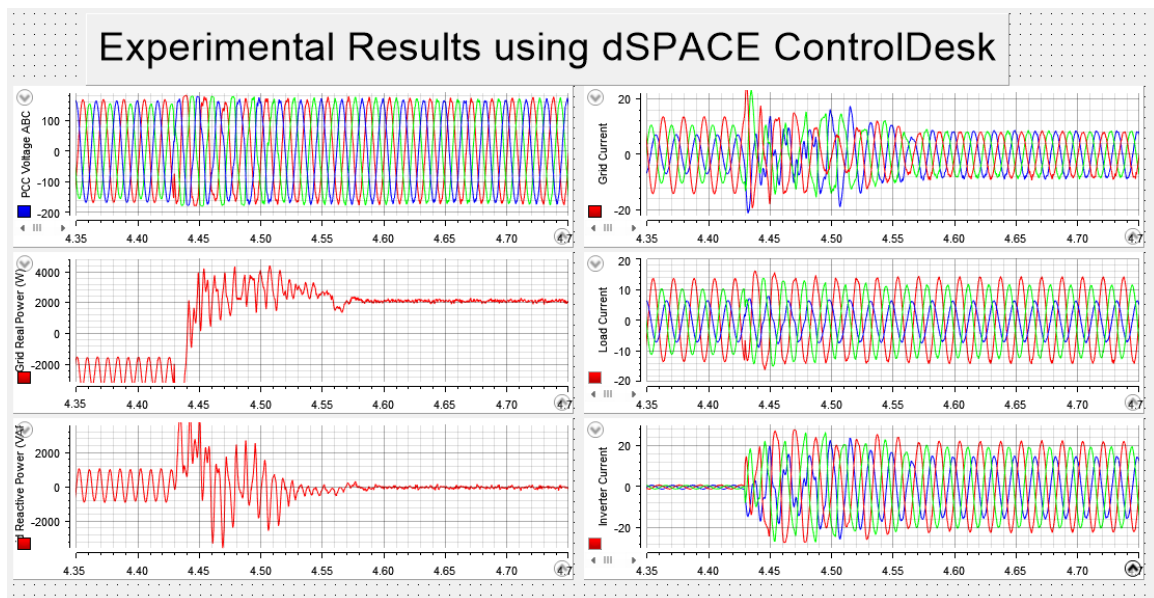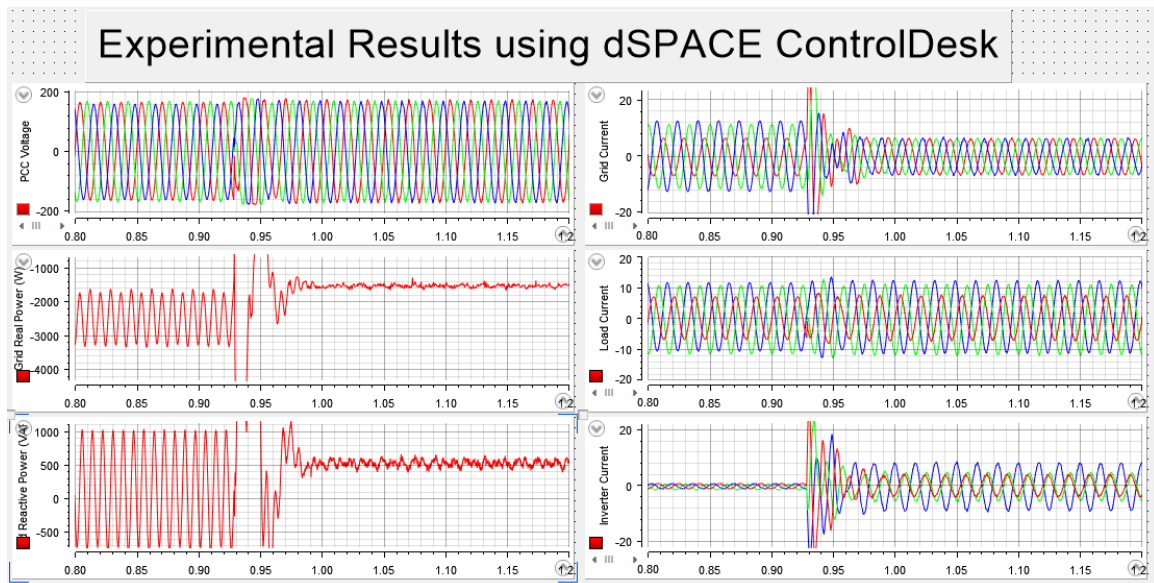

Figure 29. Hardware results using dSPACE Controldesk for real power = −1.5 kW and reactive power = 0.5 kvar under unbalanced grid inductances.
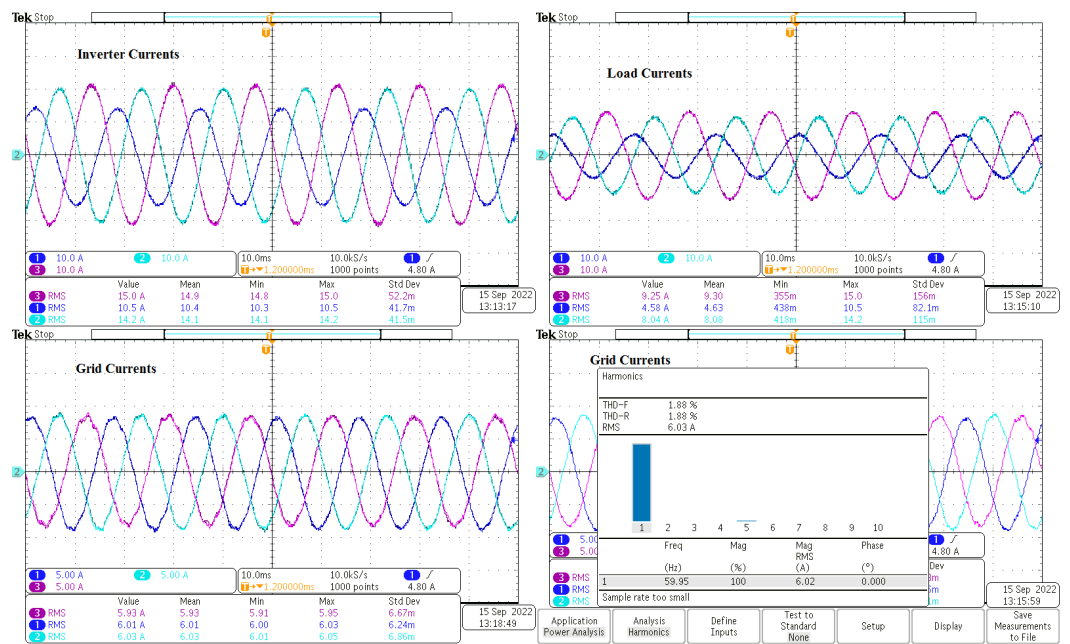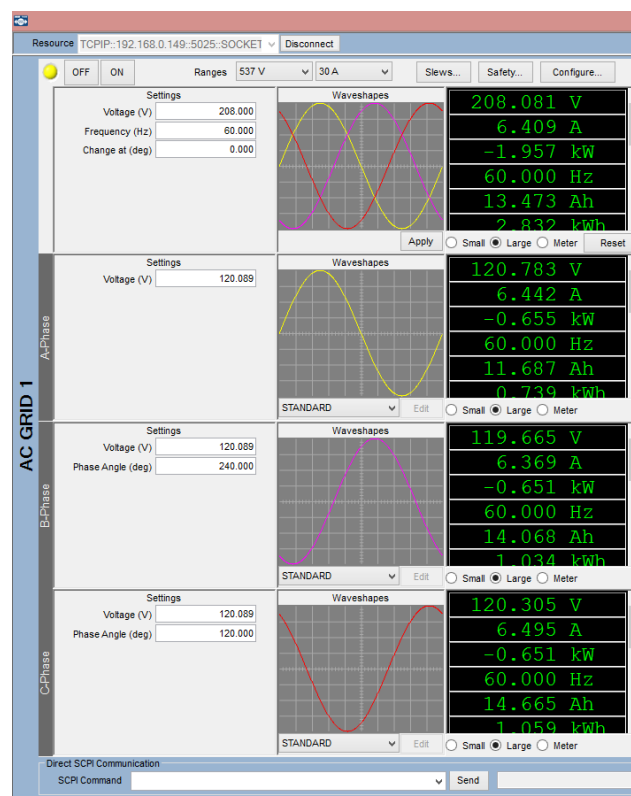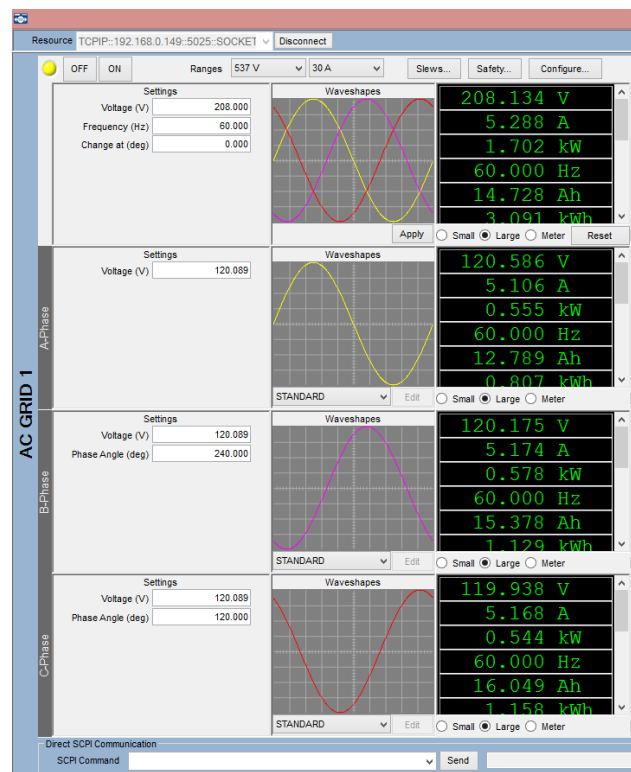

Figure 30. Hardware results using grid simulator NHR 9400 panel for real power = −1.5 kW and reactive power = 0.5 kvar under unbalanced grid inductances.

4. As seen in Figure 31, various real and reactive power values were studied. At $t = 3.5$ s, $P_{desired} = 0$ kW and $Q_{desired} = 0$ var. Then, $P_{desired} = 2$ kW at $t = 6.1$ s and $Q_{desired} = 0.5$ kvar at $t = 9.9$ s. At $t = 14.9$ s, the desired power was set to be $P_{desired} = -1.5$ kW, and at $t = 23$ s, $Q_{desired} = -0.5$ kvar.
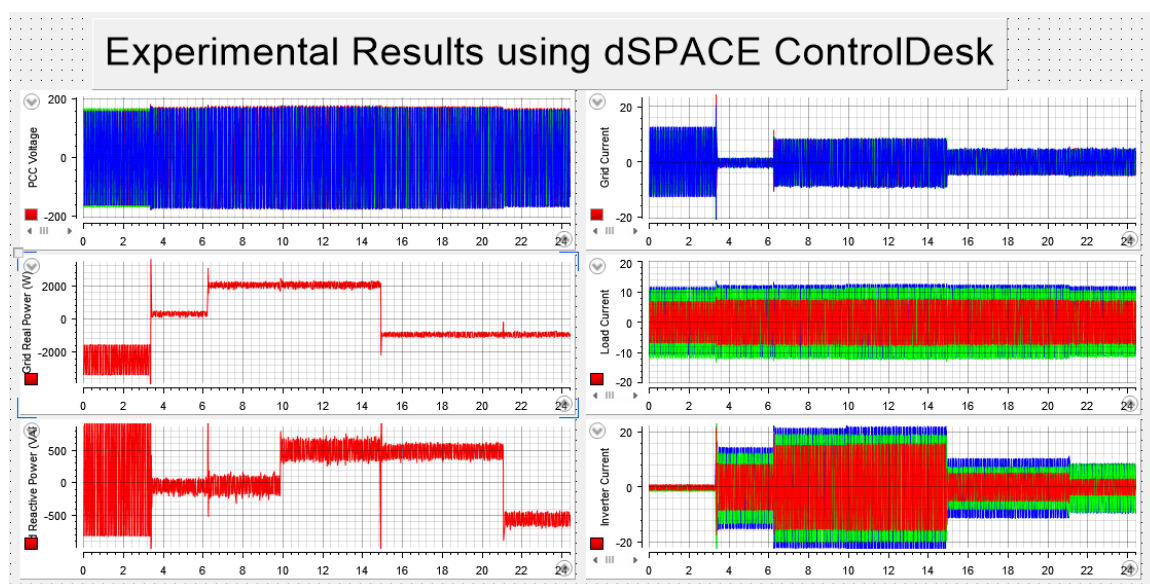
Figure 31. Hardware results of various real and reactive power values using dSPACE Controldesk under unbalanced grid inductance.

These results demonstrate that the proposed approach can control the grid's real and reactive power in both directions while balancing grid currents and PCC voltages under different unbalanced scenarios, such as an unbalanced three-phase load and unbalanced grid impedances. The large ripple in real and reactive power was reduced. Thus, the unbalanced load operation will not have an impact on other three-phase loads that are linked to the grid.

6. Conclusions

The PCC voltages and grid currents will be unbalanced under weak grid operation, where the grid impedance is taken into account. As a result, there was a significant ripple in the waveform of the real and reactive power. The other three-phase loads connected to the grid and the three-phase inverter's controller behavior are both impacted by these ripples. The bidirectional real and reactive power control technique under unbalanced grid situations is presented in this article.

The main contributions made in this article are to balance the grid currents and eliminate ripple in the real and reactive power waveforms, and perform bidirectional power regulation. The three approaches (MPRS, SCEM-P, and SCEM-PR) that were previously presented were only effective when a strong grid was considered (the grid impedance was ignored). However, this work modifies and extends the SCEM-PR by taking the advantage of the PR controller and the symmetrical component extraction method and expands them to be applicable for bidirectional power control under weak grid conditions. There is no requirement for a PLL because a conventional PR controller was used. To validate the effectiveness of the proposed methodology, various simulation and hardware results were applied under balanced and unbalanced grid impedance.

Future research can be performed in applying the proposed method to a more challenging unbalanced conditions by including nonlinear loads such as rectifiers or including a motor as a part of the load.

Author Contributions: Conceptualization, M.A., H.G. and R.M.N.; methodology, M.A.; software, M.A.; validation, M.A., H.G. and R.M.N.; formal analysis, M.A.; investigation, M.A., H.G. and R.M.N.; supervision, R.M.N. All authors have read and agreed to the published version of the manuscript.

Data Availability Statement: Not applicable.

Conflicts of Interest: The authors declare no conflict of interest.

Abbreviations

The following abbreviations are used in this manuscript:

APF	Active power filters
DDSRF PLL	Decoupled double synchronous reference frame phase-locked loop
DPD-SR	Direct phase-angle detection
EPR	Enhanced proportional-resonant controller
ESS	Energy storage systems
MPRS	Modified PR control strategy
CPT	The conservative power theory
DQ	The synchronous reference frame method
PCC	Point-of-common-coupling
PI	Proportional-integral
PLL	Phase-locked loop
PQ	The instantaneous real and reactive power theory
PR	Proportional-resonant
RES	Renewable energy resources
SAPF-UOCM	Shunt active power filter using only current measurements
SCEM	Symmetrical component extraction method
SCEM-P	Symmetrical component extraction method using P controller
SCEM-PR	Symmetrical component extraction method using PR controller

References

1. Li, P.; Dan, B.; Yong, K.; Jian, C. Research on three-phase inverter with unbalanced load. In Proceedings of the Nineteenth Annual IEEE Applied Power Electronics Conference and Exposition, Anaheim, CA, USA, 22–26 February 2004; pp. 128–133.
2. Pillay, P.; Manyage, M. Definitions of Voltage Unbalance. *IEEE Power Eng. Rev.* **2002**, *22*, 49–50. [CrossRef]
3. Guan, M.; Xu, Z. Modeling and Control of a Modular Multilevel Converter-Based HVDC System Under Unbalanced Grid Conditions. *IEEE Trans. Power Electron.* **2012**, *27*, 4858–4867. [CrossRef]
4. Tu, Q.; Xu, Z.; Chang, Y.; Guan, L. Suppressing DC voltage ripples of MMC-HVDC under unbalanced grid conditions. *IEEE Trans. Power Deliv.* **2012**, *27*, 1332–1338. [CrossRef]
5. Li, M.; Chang, X.; Dong, N.; Liu, S.; Yang, H.; Zhao, R. Arm-Current-Based Model Predictive Control for Modular Multilevel Converter Under Unbalanced Grid Condition. *IEEE J. Emerg. Sel. Top. Power Electron.* **2021**, *10*, 3195–3206. [CrossRef]
6. Choi, W.; Morris, C.; Sarlioglu, B. Modeling three-phase grid-connected inverter system using complex vector in synchronous dq reference frame and analysis on the influence of tuning parameters of synchronous frame PI controller. In Proceedings of the 2016 IEEE Power and Energy Conference at Illinois (PECI), Urbana, IL, USA, 19–20 February 2016; pp. 1–8.
7. Liu, Y.; Bai, R.; Wang, D.; Ma, W.; Wang, L. Proportional-Resonant Control Method Of Three-Phase Grid-Connected Inverter. In Proceedings of the 26th Chinese Control and Decision Conference (2014 CCDC), Changsha, China, 31 May–2 June 2014; pp. 4797–4800.
8. Kalaivani, C.; Rajambal, K. Grid Integration of Three-phase Inverter using Decoupled Double Synchronus Reference Frame PLL. In Proceedings of the 2019 International Conference on Computation of Power, Energy, Information and Communication (ICCPEIC), Piscataway, NJ, USA, 27–28 March 2019; pp. 221–226.
9. Sadeque, F.; Benzaquen, J.; Adib, A.; Mirafzal, B. Direct Phase-Angle Detection for Three-Phase Inverters in Asymmetrical Power Grids. *IEEE J. Emerg. Sel. Top. Power Electron.* **2021**, *9*, 520–528. [CrossRef]
10. Miletic, Z.; Tremmel, W.; Bründlinger, R.; Stöckl, J.; Bletterie, B. Optimal control of three-phase PV inverter under Grid voltage unbalance. In Proceedings of the 2019 21st European Conference on Power Electronics and Applications (EPE'19 ECCE Europe), Genova, Italy, 3–5 September 2019; pp. 1–11.
11. Alathamneh, M.; Yang, X.; Nelms, R.M.; Al-Gahtani, S. Power Control of a Three-phase Grid-connected Inverter using a PI Controller under Unbalanced Conditions. In Proceedings of the SoutheastCon 2022, Mobile, AL, USA, 26 March–3 April 2022; pp. 447–452.
12. Mortezaei, A.; Lute, C.; Simões, M.G.; Marafão, F.P.; Boglia, A. PQ, DQ and CPT control methods for shunt active compensators—A comparative study. In Proceedings of the IEEE Energy Conversion Congress and Exposition (ECCE), Pittsburgh, PA, USA, 14–18 September 2014; pp. 2994–3001.
13. Akagi, H.; Watanabe, E.H.; Aredes, M. *Instantaneous Power Theory and Applications to Power Conditioning*; IEEE Press/Wiley-Interscience: Hoboken, NJ, USA, 2007.
14. Marques, G.D. A comparison of active power filter control methods in unbalanced and non-sinusoidal conditions. In Proceedings of the IEEE 24th Industrial Electronics Conference, Aachen, Germany, 31 August–4 September 1998; pp. 444–449.

15. Tenti, P.; Mattavelli, P.; Paredes, H.K.M. Conservative power theory sequence components and accountability in smart grids. *Prz. Elektrotechniczny* **2010**, *6*, 30–37.

16. Al-Gahtani, S.; Nelms, R.M. A New Voltage Sensorless Control Method for a Shunt Active Power Filter for Unbalanced Conditions. In Proceedings of the 2019 IEEE International Conference on Environment and Electrical Engineering and 2019 IEEE Industrial and Commercial Power Systems Europe (EEEIC/ICPS Europe), Genova, Italy, 11–14 June 2019; pp. 1–6.

17. Al-Gahtani, S.F.; Nelms, R.M. Performance of a Shunt Active Power Filter for Unbalanced Conditions Using Only Current Measurements. *Energies* **2021**, *14*, 397. [CrossRef]

18. Alathamneh, M.; Yang, X.; Nelms, R.M.; Al-Gahtani, S. Power Control of a Three-phase Grid-connected Inverter using a Time-Domain Symmetrical Components Extraction Method under Unbalanced Conditions. In Proceedings of the IECON 2021—47th Annual Conference of the IEEE Industrial Electronics Society, Toronto, ON, Canada, 13–16 October 2021; pp. 1–6.

19. Bak, Y.; Lee, J.-S.; Lee, K.-B. Balanced Current Control Strategy for Current Source Rectifier Stage of Indirect Matrix Converter under Unbalanced Grid Voltage Conditions. *Energies* **2017**, *10*, 27. [CrossRef]

20. Mohammed, N.; Ciobotaru, M.; Town, G. Online Parametric Estimation of Grid Impedance Under Unbalanced Grid Conditions. *Energies* **2019**, *12*, 4752. [CrossRef]

21. Chen, X.; Wu, W.; Gao, N.; Liu, J.; Chung, H.S.-H.; Blaabjerg, F. Finite Control Set Model Predictive Control for an LCL-Filtered Grid-Tied Inverter with Full Status Estimations under Unbalanced Grid Voltage. *Energies* **2019**, *12*, 2691. [CrossRef]

22. Alharbi, M.; Isik, S.; Alkuhayli, A.; Bhattacharya, S. Power Ripple Control Method for Modular Multilevel Converter under Grid Imbalances. *Energies* **2022**, *15*, 3535. [CrossRef]

23. Yu, Y.; Wang, Z.; Wan, X. Optimal Current Balance Control of Three-Level Inverter under Grid Voltage Unbalance: An Adaptive Dynamic Programming Approach. *Energies* **2019**, *12*, 2864. [CrossRef]

24. Ma, W.; Ouyang, S.; Xu, W. Improved Frequency Locked Loop Based Synchronization Method for Three-Phase Grid-Connected Inverter under Unbalanced and Distorted Grid Conditions. *Energies* **2019**, *12*, 1023. [CrossRef]

25. Wang, S.; Bao, D.; Gontijo, G.; Chaudhary, S.; Teodorescu, R. Modeling and Mitigation Control of the Submodule-Capacitor Voltage Ripple of a Modular Multilevel Converter under Unbalanced Grid Conditions. *Energies* **2021**, *14*, 651. [CrossRef]

26. Tan, K.-H.; Lin, F.-J.; Chen, J.-H. A Three-Phase Four-Leg Inverter-Based Active Power Filter for Unbalanced Current Compensation Using a Petri Probabilistic Fuzzy Neural Network. *Energies* **2017**, *10*, 2005. [CrossRef]

27. Shin, H.; Chae, S.H.; Kim, E.-H. Unbalanced Current Reduction Method of Microgrid Based on Power Conversion System Operation. *Energies* **2021**, *14*, 3862. [CrossRef]

28. Nakadomari, A.; Shigenobu, R.; Kato, T.; Krishnan, N.; Hemeida, A.M.; Takahashi, H.; Senjyu, T. Unbalanced Voltage Compensation with Optimal Voltage Controlled Regulators and Load Ratio Control Transformer. *Energies* **2021**, *14*, 2997. [CrossRef]

29. Najafi, F.; Hamzeh, M.; Fripp, M. Unbalanced Current Sharing Control in Islanded Low Voltage Microgrids. *Energies* **2018**, *11*, 2776. [CrossRef]

30. Kim, J.-M.; Song, G.-S.; Jung, J.-J. Zero-Sequence Voltage Injection Method for DC Capacitor Voltage Balancing of Wye-Connected CHB Converter under Unbalanced Grid and Load Conditions. *Energies* **2021**, *14*, 1019. [CrossRef]

31. Ahmed, E.M.; Aly, M.; Elmelegi, A.; Alharbi, A.G.; Ali, Z.M. Multifunctional Distributed MPPT Controller for 3P4W Grid-Connected PV Systems in Distribution Network with Unbalanced Loads. *Energies* **2019**, *12*, 4799. [CrossRef]

32. Cai, H.; Zhang, P.; Zhao, H.; Shi, J.; Yao, W.; He, X. Controller design for three-phase inverter with power unbalanced loads applied in microgrids. In Proceedings of the 2015 IEEE Energy Conversion Congress and Exposition (ECCE), Montreal, QC, USA, 20–24 September 2015; pp. 4588–4593.

33. Alathamneh, M.; Yang, X.; Nelms, R.M. Power Control of a Three-phase Grid-connected Inverter using a Proportional-Resonant Control Method under Unbalanced Conditions. In Proceedings of the IECON 2021—47th Annual Conference of the IEEE Industrial Electronics Society, Toronto, ON, Canada, 13–16 October 2021; pp. 1–6.

34. Alathamneh, M.; Ghanayem, H.; Yang, X.; Nelms, R.M. PR Controller for a Three-phase Grid-connected Inverter in an Unbalanced System using a Time-Domain Symmetrical Components Extraction Method. In Proceedings of the 2022 IEEE 31st International Symposium on Industrial Electronics (ISIE), Anchorage, AK, USA, 1–3 June 2022; pp. 18–23.

35. Pereira, L.F.A.; Bazanella, A.S. Tuning Rules for Proportional Resonant Controllers. *IEEE Trans. Control. Syst. Technol.* **2015**, *23*, 2010–2017. [CrossRef]

36. Akagi, H.; Kanazawa, Y.; Nabae, A. Instantaneous reactive power compensators comprising switching devices without energy storage. *IEEE Trans. Ind. Appl.* **1984**, *20*, 625–630. [CrossRef]

37. Duesterhoeft, W.C.; Schulz, M.W.; Clarke, E. Determination of Instantaneous Currents and Voltages by Means of Alpha, Beta, and Zero Components. *Trans. Am. Inst. Electr. Eng.* **1951**, *70*, 1248–1255. [CrossRef]

38. Yang, X.; Alathamneh, M.; Nelms, R.M. Improved LCL Filter Design Procedure for Grid-Connected Voltage-Source Inverter System. In Proceedings of the 2021 IEEE Energy Conversion Congress and Exposition (ECCE), Vancouver, BC, Canada, 10–14 October 2021; pp. 3587–3591.